SCIENCE CHINA
Information Sciences

• LETTER •

August 2021, Vol. 64 189403:1–189403:3
https://doi.org/10.1007/s11432-020-3098-x

Controlled nano-cracking actuated by an in-plane voltage

Qiang LUO, Zhe GUO, Shuai ZHANG, Xiaofei YANG, Xuecheng ZOU, Jeongmin HONG & Long YOU*

School of Optical and Electronic Information, Huazhong University of Science and Technology, Wuhan 430074, *China*

Received 23 April 2020/Revised 6 July 2020/Accepted 10 October 2020/Published online 21 May 2021

Citation Luo Q, Guo Z, Zhang S, et al. Controlled nano-cracking actuated by an in-plane voltage. Sci China Inf Sci, 2021, 64(8): 189403, https://doi.org/10.1007/s11432-020-3098-x

Dear editor,

Cracking has been generally regarded as an undesirable phenomenon to be avoided owing to their highly stochastic process and irreversibility. However, to induce nanocracks deliberately has been widely investigated because of their great potential for extended applications, such as strain sensors [1], flexible electronics [2] and nano-fabrication [3]. Recently, electrically switchable nanocracks in ferroelectrics have been experimentally verified [4], which offers great promise for novel energy-efficient memory applications.

However, such device layout needs further refining owing to the randomly distributed cracks in a continuous alloy thin film (see Appendix A). More recently, a viable approach to precisely control such nanocracks is to pattern the alloy thin film into a "bridge-like" structure to regulate the electric-field distribution, thereby the crack initiation can be confined within the certain regions with the highest values of electric-field [5]. Nevertheless, a large out-of-plane voltage is required to generate and manipulate such a nanocrack in a bulk ferroelectric oxide since the fact that the control voltage depends on the distance between the top and bottom electrodes [6].

Here, we utilize a low in-plane voltage to induce and manipulate the nanocracks in ferroelectric oxide and construct two types of devices, including non-volatile switching of single-crack and complementary switching of two-crack. The full experimental details and analytical methods are shown in Appendix B. More importantly, the in-plane control voltage can be easily reduced by decreasing the gap width between two separated electrodes. Compared with the conventional NEM switches based on cantilever [7], such ferroelectric crack-based devices not only have a simpler structure and easier fabrication process, but also provide a simple way to achieve energy-efficient and high-density electronic applications, such as reconfigurable logic (RL).

Non-volatile switching of single-crack. Based on the "bridge-like" structure, the nanocrack can be induced in the central MnPt strip by applying an in-plane voltage. The crack generation process can be found in Appendix C. The non-volatile open and closed states of crack are shown in Figure 1(a). As shown in Figure 1(a)I, when $V_{\rm C}$ varies from -40 to 0 V, the crack keeps open state and blocks the current path in the MnPt strip, resulting in a high-resistance state (HRS). Conversely, the MnPt strip recovers back to metallic contact and leads to a low-resistance state (LRS) after sweeping $V_{\rm C}$ from +40 to 0 V, corresponding to a closed state of crack (Figure 1(a)II).

The transfer characteristics of the crack are shown in Figure 1(a)III. When $V_{\rm C} = 0$ V, the crack is closed, corresponding to a saturated channel current ($I_{\rm sd}$) of 4 μA. After sweeping $V_{\rm C}$ from 0 to -16 V, the crack opens and induces a sharp decrease of $I_{\rm sd}$ to 1 nA (arrow 1). Further, $I_{\rm sd}$ remains the minimum value when $V_{\rm C}$ reduces to -40 V and then returns to 0 V, illustrating a nonvolatile open-state (arrow 2). Subsequently, as represented by arrow 3, $I_{\rm sd}$ dramatically increases to the saturated value when $V_{\rm C}$ increases from 0 to +16 V. Finally, $I_{\rm sd}$ remains unchanged as $V_{\rm C}$ increases to + 40 V and recovers back to 0 V (arrow 4). When $V_{\rm C}$ is repeatedly scanned up to 10 times, the results show similar square curves, which demonstrates a good repeatability. In addition, Figure 1(a)IV shows the ferroelectric leakage current ($I_{\rm L}$) during sweeping the $V_{\rm C}$. Obviously, the $I_{\rm L}$ exhibits two distinct peaks at the switching voltage, which indicates the ferroelectric domain switching [8]. Therefore, the in-plane voltage actuated switching of the crack should also be related to the ferroelectric domain switching.

Complementary switching of two-crack. Such device merely comprises two separated triangular MnPt electrodes deposited on PMN-PT substrate. Crack generation process and crack characterization are given in Appendix D. As shown in Figure 1(b)I, under $V_{\rm C} = +50$ V, the crack in the upper area (crack-1) opens while the crack in the lower area (crack-2) closes (nearly disappeared). Conversely, when $V_{\rm C}$ is -50 V, the crack-1 closes and crack-2 opens (Figure 1(b)II).

Furthermore, the complementary $I_{\rm sd}$-$V_{\rm C}$ loops of these two cracks are shown in Figure 1(b)III. At the initial state

* Corresponding author (email: lyou@hust.edu.cn)

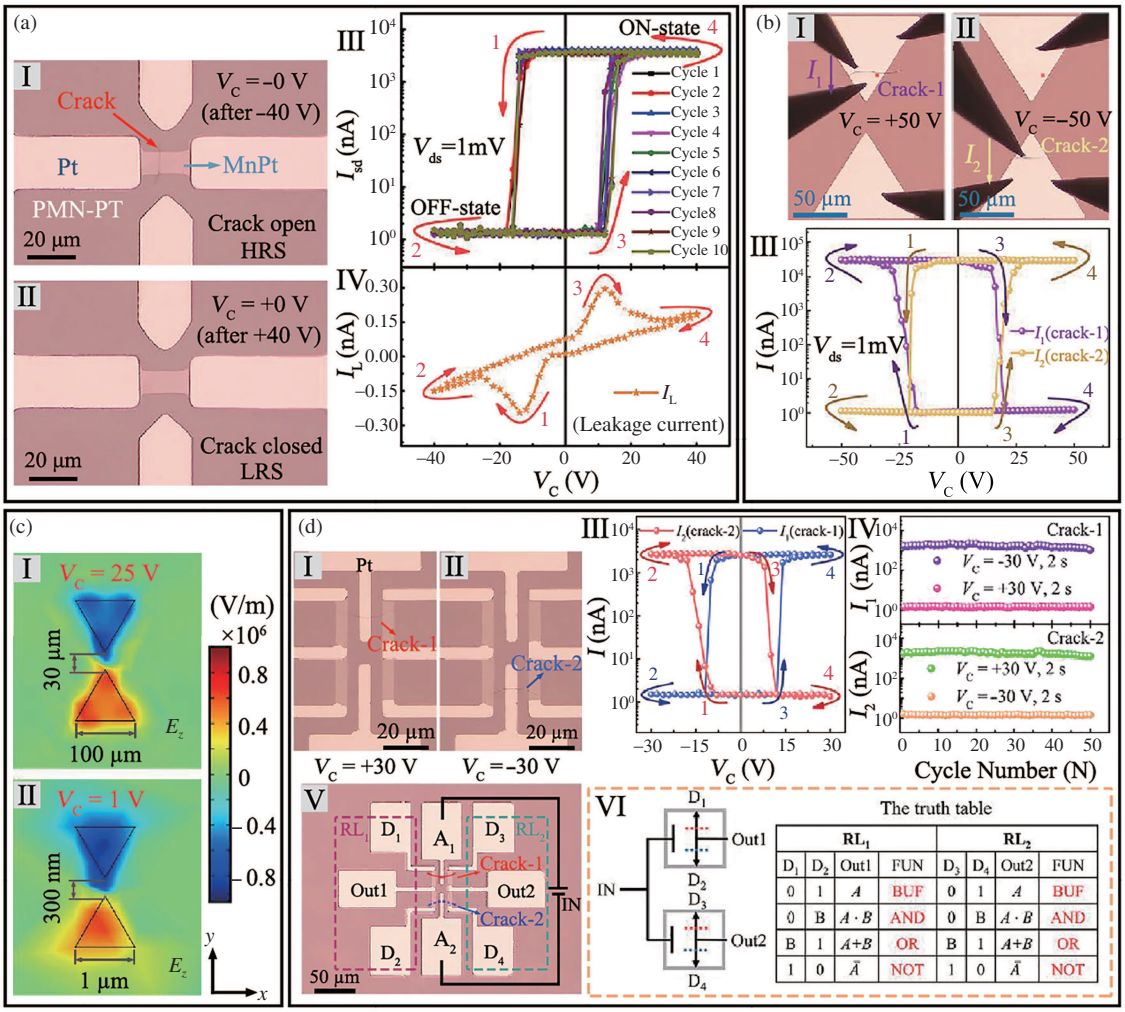

RL_1				RL_2			
D_1	D_2	Out1	FUN	D_3	D_4	Out2	FUN
0	1	A	BUF	0	1	A	BUF
0	B	$A \cdot B$	AND	0	B	$A \cdot B$	AND
B	1	$A+B$	OR	B	1	$A+B$	OR
1	0	$\bar{A}$	NOT	1	0	$\bar{A}$	NOT

Figure 1 (Color online) (a) Non-volatile switching of single-crack: (I) and (II) the open and closed state of the single-crack after scanning V_C; (III) the repeated I_{sd}-V_C loops of the single-crack based device; (IV) the corresponding switching leakage current (I_L) in the PMN-PT substrate. (b) Complementary switching of two-crack: (I) and (II) the optical images of these two cracks (crack-1 and crack-2) in opposite states, respectively; (III) the complementary resistive switching I-V_C characteristics; (c) complementary switching mechanism of crack under an in-plane voltage: verification from COMSOL simulation that the complementary E_z distributions of the devices with a gap width of 30 μm (I) and 300 nm (II), respectively. (d) Reconfigurable logic (RL) implemented by complementary extended two cracks: (I) and (II) the optical images of complementary two cracks under V_C; (III) the complementary resistive switching I-V_C characteristics; (IV) the repeatability test for the complementary switching; (V) the diagram of RL unit through programmable signal routing; (VI) the circuit symbol of RL and the corresponding truth table.

of $V_C = 0$ V, I_1 approaches to 1 nA while I_2 reaches the saturate value of 30 μA, indicating an open/closed state of crack-1/crack-2. Further, as V_C sweeps from 0 to −25 V, I_1 suddenly increases to 30 μA while I_2 dramatically decreases to 1 nA, demonstrating complementary switching behaviors (indicated by arrow 1). Conversely, reversely increasing V_C from 0 to +25 V will bring these two cracks to their initial state (represented by arrow 3). The subsequent increase of V_C to +50 V and back to 0 V does not change the state, also demonstrating a nonvolatile switching characteristic.

Mechanism of crack complementary switching. As mentioned in previous studies, the crack in such heterostructure was induced by the microscopic strain at domain boundaries, originating from the interaction between electrically switchable domains and defect-pinned domains [4,5,8]. Therefore, the crack formation and switching should also be attributed to the electric-field actuated domain switching. To further investigate the complementary switching mechanism of cracks, the x-, y- and z- components of electric-field (E_x, E_y and E_z) are analyzed by COMSOL simulation. As shown in Figure 1(c)I, the opposite directions of the simulated E_z distributions indicate a good agreement with the experimental results of the complementary switching of cracks. More analysis results are given in Appendix E. Therefore, the complementary switching of cracks should be attributed to the complementary E_z distribution. Moreover, Figure 1(c)II also shows complementary E_z distributions with a gap width of 300 nm, suggesting that such a crack-based device can still work when the device size shrinks.

Application for energy-efficient and high-density RL. In our design, RL function can be easily implemented by employing a two-crack based device with separated input and output points. The device structure and electrical measurement geometry are illustrated in Appendix F. Under V_C, crack-1 in the upper electrode (Figure 1(d)I) and crack-2 in the lower electrode (Figure 1(d)II) are generated in succes-

sion, and then propagate through the left and right MnPt strips. The transfer characteristic in Figure 1(d)III illustrates a similar complementary switching of cracks opening and closing. In addition, under alternating voltage pulses, the complementary switching can be cycled dozens of times without performance degradation (Figure 1(d)IV).

Furthermore, such crack-based device can be used to implement a complex RL function. Figure 1(d)V shows the diagram of the RL unit with programmable signal routings. The input voltage (IN) applied between two separated electrodes (A_1 and A_2) is used to manipulate the complementary switching of cracks, which would also drive the complementary switching of the lateral MnPt strips. The output signals (Out1 and Out2) contact one of two supply data signals (D_1/D_2 and D_3/D_4), respectively, depending on the states of crack-1 and crack-2. Two RL units (RL_1 and RL_2) can be easily realized within only one device owing to a symmetrical structure. The simplified circuits symbol for the reconfigurable circuits is shown in Figure 1(d)VI. Based on such structure, any two logic functions can be implemented independently. For instance, the basic logic functions such as BUF, AND, OR and NOT can be implemented in a single device through programming the data signals D_1/D_2 (D_3/D_4), as described by the truth table. Compared with the conventional CMOS-based RL circuits, such crack-based device has a simper structure, and could also offer sizeable advantages in areal logic density and operational energy.

Conclusion. Herein, we have demonstrated a controllable nano-cracking in MnPt/PMN-PT heterostructures by applying a small in-plane voltage onto two separated electrodes. Based on such ferroelectric cracking, non-volatile switching of single-crack and complementary switching of two-crack were realized in a simple manner, combining the advantages of both NEM switch and ferroelectric. In addition, the complementary switching of cracks is mainly decided by the complementary E_z distribution. Finally, RL implemented by complementary switching of two cracks has been demonstrated. The current work unveils a unique device platform, giving rise to multiple energy-efficient and high-density integrated applications.

Acknowledgements This work was supported by National Natural Science Foundation of China (Grant Nos. 62074063, 61904060, 61821003, 61674062), National Key Research and Development Program of China (Grant No. 2020AAA0109000), Research Project of Wuhan Science and Technology Bureau (Grant No. 2019010701011394), and Fundamental Research Funds for the Central Universities (Grant No. HUST: 2018KFYXKJC019).

Supporting information Appendixes A–F. The supporting information is available online at info.scichina.com and link.springer.com. The supporting materials are published as submitted, without typesetting or editing. The responsibility for scientific accuracy and content remains entirely with the authors.

References

1 Kang D, Pikhitsa P V, Choi Y W, et al. Ultrasensitive mechanical crack-based sensor inspired by the spider sensory system. Nature, 2014, 516: 222–226
2 Zhao Q, Wang W J, Shao J Y, et al. Nanoscale electrodes for flexible electronics by swelling controlled cracking. Adv Mater, 2016, 28: 6337–6344
3 Nam K H, Park I H, Ko S H. Patterning by controlled cracking. Nature, 2012, 485: 221–224
4 Liu Z Q, Liu J H, Biegalski M D, et al. Electrically reversible cracks in an intermetallic film controlled by an electric field. Nat Commun, 2018, 9: 41
5 Luo Q, Guo Z, Huang H B, et al. Nanoelectromechanical switches by controlled switchable cracking. IEEE Electron Device Lett, 2019, 29: 131–133
6 Íñiguez J, Zubko P, Luk'yanchuk I, et al. Ferroelectric negative capacitance. Nat Rev Mater, 2019, 4: 243–256
7 Lee J O, Song Y H, Kim M W, et al. A sub-1-volt nanoelectromechanical switching device. Nat Nanotech, 2013, 8: 36–40
8 Luo Q, Guo Z, Zhang S, et al. Crack-based complementary nanoelectromechanical switches for reconfigurable computing. IEEE Electron Device Lett, 2020, 41: 784–787